IBRO Reports 6 (2019) 18–30

Contents lists available at ScienceDirect

IBRO Reports

journal homepage: www.elsevier.com/locate/ibror

Research Paper

The impact of age on number and distribution of proliferating cells in subgranular zone in adult mouse brain

Karen Smith[a], Mikhail V. Semënov[a,b,*]

[a] New England Geriatric Research Education and Clinical Center, Bedford Division, Edith Nourse Rogers Memorial Veterans Hospital, Bedford, MA, United States
[b] The Department of Pathology and Laboratory Medicine, Boston University School of Medicine, Boston, MA, United States

ARTICLE INFO

Keywords:
Adult neurogenesis
Dentate gyrus
Subgranular zone
Neural precursors
Aging
Adult mouse brain
Mouse
Point cloud

ABSTRACT

The mouse brain retains an ability to produce hippocampal granule neurons during the mouse's entire lifespan. The neurons are produced in the subgranular zone (SGZ) located on the inner surface of the granule cell layer in the dentate gyrus (DG). In our study, we used a point cloud approach to characterize how the production and distribution of neural precursors for new hippocampal neurons change in the mouse brain relative to age. We found that the production of neural precursors decreases 64 fold from the age of 30 days to the age of 2.5 years. Within the SGZ the decline of cell proliferation continues during entire mouse life. We reconstructed the distribution of proliferating cells along the longitudinal axis of the SGZ and found that the highest number of proliferating cells are located approximately 0.75 mm from the dorsomedial end of the SGZ that corresponds to the most dorsal part of the DG in the mouse brain. The distribution of proliferating cells in the SGZ showed no apparent aggregations, periodicity or any other readily identifiable spatial characteristics. Proliferating cells in the SGZ tended to be located separately from other proliferating cells. About two thirds of them have no closely located other proliferating cells, and the remaining third is located in small clusters comprised of 2 or 3 proliferating cells. Based on our measurements, we calculated that from the age of 30 days to the age of 2.5 years 1.5 million neural precursors are produced in the SGZ.

Introduction

New hippocampal neurons are produced in the adult mouse brain. The production is strictly limited to new granule cells in the dentate gyrus (Balu and Lucki, 2009; Gonçalves et al., 2016; Ihunwo et al., 2016). Precursors for new neurons are produced in the SubGranular Zone (SGZ) located on the inner surface of the dentate gyrus granule cell layer. After production, the precursors migrate a short distance from the SGZ into the granule cell layer where they differentiate into neurons and are incorporated into existing neural circuitry in the hippocampus (Balu and Lucki, 2009; Ming and Song, 2011; Gonçalves et al., 2016).

The SGZ contains neural stem cells (NSCs). The identity of these cells is still not entirely clear, but the radial glia-like (RGL) cells are plausible candidates for this role (Seri et al., 2001). These cells resemble the radial glia cells that serve as embryonic NSCs in the developing mouse brain. The RGL cells produce neural precursors (Kriegstein and Alvarez-Buylla, 2009; Bonaguidi et al., 2011). These precursors may go through additional rounds of cell division and after that they differentiate and incorporate into the DG as new neurons or astrocytes (Bonaguidi et al., 2011; Kempermann et al., 2015). Only a small portion of progenitors complete this transition, and the majority of them are eliminated via programmed cell death (Biebl et al., 2000). New neurons show increased activity and plasticity and are thought to play an important role in hippocampal functioning (Gonçalves et al., 2016).

Hippocampal neurogenesis in mice responds to many environmental stimuli. Physical exercise stimulates neural precursor production (van Praag et al., 1999), and an enriched environment increases survival of new neurons (Kempermann et al., 1997a). In contrast, chronic stress decreases precursor production (Mirescu and Gould, 2006). These changes show that adult neurogenesis could be playing a role in the mouse adaptation to new environmental conditions. New neurons contribute to several hippocampal functions. The best studied are spatial learning and memory (Deng et al., 2010; Aimone et al., 2011). This could open a possibility to adjust these functions by altering adult neurogenesis. Since hippocampal neurogenesis is found in humans, studies in mice are relevant to human health (Ihunwo et al., 2016).

In contrast to significant progress in our understanding of molecular mechanisms of the regulation of adult neurogenesis, there is limited

* Corresponding author at: NE GRECC, Bedford VAMC, Building 18, 200 Springs Rd, Bedford, MA 01730, USA.
E-mail address: mikhail.semenov@va.gov (M.V. Semënov).

https://doi.org/10.1016/j.ibror.2018.12.002
Received 8 October 2018; Accepted 7 December 2018

information available about the spatial organization of neural precursor production in the SGZ. Therefore, we report how neural precursor production is distributed in the SGZ and how it changes with mouse aging increase.

Experimental procedures

Ethics statement

All experiments with mice, including euthanasia, meet AVMA guidelines and were conducted following NIH and international guidelines and with veterinarian supervision. All experimental procedures were approved by The Institutional Animal Care and Use Committee (Department of Veterans Affairs, ENRM VA Hospital IACUC, Protocol SE-08-13-96).

Animals and tissue collection

C57BL/6 J male mice were purchased from The Jackson Laboratory (Bar Harbor, ME, USA) and the 2.5 year old mice were provided by the Institute of Aging (NIH) from the aging mice collection. The two mice per age group are listed in Table 1. Mice were injected intraperitoneally with 50 mg/kg 5-Ethynyl-2´-deoxyuridine (EdU) (Invitrogen, CA, USA), euthanized one hour after injection, and transcardially perfused first with 20 ml of cold PBS with 10 U/ml of heparin and then with 120 ml of cold PBS with 4% formaldehyde. Brains were extracted and incubated in PBS with 4% formaldehyde at + 4 °C for a day and then transferred into 100 mM phosphate buffer, pH 7.4, with 20% glycerol and 2% DMSO for at least two days before cutting.

Immunohistochemistry

The processing and staining of mouse brain sections were performed as described in our previous publication (Bordiuk et al., 2014). Mouse brains were cut serially at 50 μm through the entire extent of the brain using a freezing sledge microtome. Sections were collected in a 24-well plate with wells filled with tris-buffered saline (TBS, pH7.5). Transverse sectioning was used because the shape of the section is better maintained during the staining and mounting procedures which simplified the virtual reconstruction using the images of all sections of the mouse brain. Sections were first permeabilized using free-float incubation in a TBS solution with 0.5% triton-X100 for one hour at room temperature on a rocker table with gentle agitation. Sections were then transferred directly into the EdU Alexa 647 staining solution containing EdU staining buffer, $CuSO_4$, Alexa Fluor 647 azide and ascorbic acid in a proportion recommended by the manufacturer (Thermo Fisher Scientific, catalog# C10340) and incubated in the dark for one hour. Sections were then well washed in PBS (3 x 10 min), and all sections from each well were mounted on one gelatin coated microscope slide (25 mm x 75 mm) and air dried. Slides were coverslipped using a 5% propyl gallate/glycerol mounting media with DAPI and sealed with black nail polish.

Microscopy and image analysis

Image acquisition and analysis were performed as described previously (Bordiuk et al., 2014). Each microscope slide was scanned using the Zeiss AxioImagerZ2 microscope with a EC Plan-NEOFLUAR 5X/0.16 objective. We used a 5X objective for image acquisition because its focal depth (54.84 μm at 690 nm) exceeds the thickness of brain sections (after air drying, mounted 50 μm brain sections become approximately 25–27 μm thin) and the spatial resolution (1.29 μm X 1.29 μm per pixel) is sufficient for unambiguous detection of EdU-labeled nuclei. Each scan produced a 16-bit composite image of the entire microscope slide consisting of 600 individual images. Composite images were stitched, images for individual section were cut out, arranged in the order according to their position in the brain and manually registered (Bordiuk et al., 2014). We counted the number of all EdU-labeled nuclei in on all brain sections using the Find Maxima Process with the tolerance parameter set to 1500 (Fiji image processing package) and obtained coordinates for each EdU-labeled nucleus. The tolerance parameter was set to 1500 because this allowed us to automatically identify all visually detectable EdU-labeled nuclei and at the same time had a low rate of false positive identifications that we manually removed. EdU-labeled nuclei identified on each brain section were placed in one horizontal plane. The dorsoventral distance between the planes produced for two neighbouring sections was set to be equal to the section thickness, 50 μm. Thus, each reconstructed SGZ was presented as a distribution of EdU-labeled nuclei in about 80 horizontal planes which corresponds to the number of brain sections used for the reconstruction.

We used brain sections of a 120 day old mouse that was not injected with EdU as the negative control. The staining of these sections for EdU did not reveal any EdU stained nuclei and the Find Maxima Process had not identified any EdU positive nuclei on images of these sections.

To distinguish proliferating cells located in the SGZ we manually selected all EdU-labeled nuclei located within 20 μm from the inner surface of the granular cell layer. We selected and counted EdU-labeled nuclei in the SGZ on all mouse brain sections that cut across the SGZ.

Data analysis

Microsoft Excel was used for all data analysis and chart drawing. Adobe Photoshop and Microsoft PowerPoint were used for figure preparation.

To calculate the local number density for each EdU-labeled nucleus in the SGZ, we calculated the distances between each EdU-labeled nucleus and all other EdU-labeled nuclei in the SVZ using the nuclei coordinates and then counted how many of them were located closer than 200 μm to this nucleus. Such an approach is applicable to our data even if all EdU-labeled nuclei on each brain section is located in one plane. The difference is that in our case we are counting the number of EdU-labeled nuclei located in a series of cylinders stacked on top of each other rather than inside the sphere with a 200 μm radius. The height of all cylinders is equal to the section thickness, 50 μm, and the radius is equal to the radius of the circle that the sphere creates when it crosses each plane with the nuclei. The total volume of all these cylinders produced by the intersection of the sphere with the planes is only 1.5% smaller than the volume of the sphere. Thus, by using this approach we are counting the number of EdU-labeled nuclei in a volume that is practically equal to the volume of the sphere. To calculate the number of EdU-labeled nuclei inside the 50 μm sphere surrounding each nucleus, we calculated the number of EdU-labeled nuclei located closer than 52.5 μm to each nucleus. This allows us to count the number of EdU-labeled nuclei in the volume that is only 2% smaller than the volume of 50 μm sphere.

To virtually transform the distribution of proliferating cells in the SGZ and represent it as a flat surface, we established a three-dimensional tracing of the hilus apex for the left and right dentate gyrus in the brain of 60D-A mouse. Next we placed points on these tracings with 50 μm intervals and determined their coordinates. Then we found the perpendicular distance (the shortest distance) from each proliferating cell to the placed points. To visualize the distribution of proliferating cells we showed the hilus tracing as a straight line and each proliferating cell as a black dot. The position of each proliferating cell on the flattened SGZ was defined by its location on the external or internal SGZ arm and the position along the hilus tracing and the distance from the tracing.

Statistical analyses were performed using a one-way analysis of variance (ANOVA) with a post-hoc two-tailed Student's *t*-test with significance set at $p < 0.05$. The preliminary analysis shows that age has an extremely large effect on the number of proliferating cells in the SGZ with Cohen's D routinely exceeding 10 between measurements for two

consecutive age points. In such circumstances a *t*-test can be reliably applied to evaluate the significance of the difference between measurements with sample size n = 2 (de Winter, 2013).

Data availability

All data generated or analysed during this study are included in this published article.

Results

We analysed the brains of 30, 60, 120, 240 day and 1 and 2.5 year old mice to find how the number and distribution of proliferating cells change in the SGZ relative to aging. For each age group we analysed two mice (Table 1). The average difference between the numbers of detected proliferating cells in the SGZ was about 2.5% showing good repeatability of our detection technique.

Table 1
Age-related decrease in the number and average volume number density of proliferating cells located in the SGZ.

Mouse	Mouse age	SGZ	
		Number of EdU labeled nuclei	Average local number density
30D-A	30 days	4526	63.6
30D-B	30 days	4493	69.9
60D-A	60 days	2732	39.4
60D-B	60 days	2570	35.2
120D-A	120 days	1554	21.5
120D-B	120 days	1581	20.1
240D-A	240 days	625	11.2
240D-B	240 days	613	10.8
1Y-A	1 year	314	6.1
1Y-B	1 year	325	7.3
2.5Y-A	2.5 years	69	2.0
2.5Y-B	2.5 years	70	1.5

We cut entire mouse brains transversely, stained all sections for EdU, and counted all cells in the SGZ with EdU stained nuclei in all sections of all analysed mouse brains. Some EdU labelled nuclei in the SGZ could be cut across in the process of brain sectioning, and consequently their fragments would be present on two consecutive sections. Counting both fragments would lead to the overcounting of the number of proliferating cells in the SGZ. To evaluate how many such cut nuclei are present on brain sections, we overlay images of consecutive sections of a 120 day old mouse (120D-A), count all EdU stained nuclei and identify among them pairs that are located in the same position on both sections (Fig. 1A). We analysed areas of the brain with a low density of proliferating cells to simplify identification of such nuclei. We counted 617 EdU labelled nuclei on 7 consecutive sections and identified only 4 pairs of nuclei that were located in same position on two consecutive sections and possibly representing two parts of one cut nucleus.

Granule cells in the DG form two symmetrical arches on the left and right side of the mouse brain in the posterior half of the telencephalon (Fig. 1B). Proliferating cells in the SGZ are located on the inner surface of the granule cell layer. To distinguish these cells we manually selected them (Bordiuk et al., 2014) and obtained their coordinates. Proliferating cells are quite abundant in the dorsal part of the SGZ in young mice. However, their number substantially decreases towards the middle portion of the SGZ and the most ventral part of the SGZ appears to be almost devoid of proliferating cells (Figs. 1B, 2). In whole, the distribution of proliferating cells in the SGZ shows no apparent aggregations, periodicity or any other readily identifiable spatial characteristics (Fig. 2).

We counted the number of EdU labelled nuclei in the SGZ and calculated their average local number density in each analysed mouse

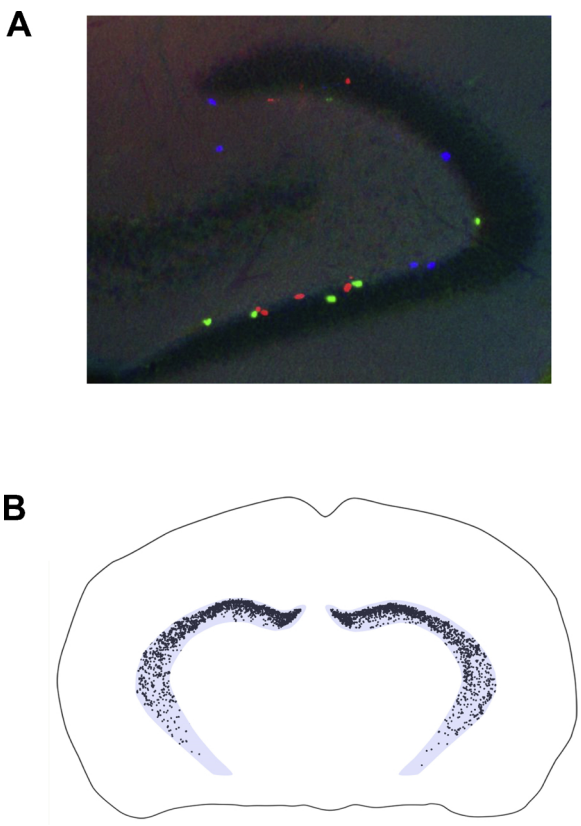

Fig. 1. More proliferating cells are located in the dorsal part SGZ than in the ventral part.
(**A**). The distribution of EdU-labelled nuclei in three consecutive sections #60, #61, and #62 of the mouse brain 120B-A. The fragment of three consecutive registered sections includes the DG on the right side of the brain that could be seen as a dark silhouette. EdU-labelled nuclei in section #60 are shown in red, in section #61 in green, and in section #62 in blue. EdU-labelled nuclei located on these three sections at different locations and no overlaps are observed amongst them.
(**B**). More proliferating cells are located in the dorsal part SGZ than in the ventral part. Coronal view. Each EdU-labelled nucleus is shown as a black dot. The granule cell layer is shown schematically in blue. The brain shape is outlined with a black line.

brain. The local number cell density for each EdU stained nuclei in the SGZ was calculated by counting how many other EdU stained nuclei are located closer than 200 μm to this nucleus. We detected 4500 proliferating cells with the average local number cell density of 67 in the SGZ of 30 day old mice (Table 1). These numbers decrease by 40%, from 4500 to about 2650 and from 67 to 37 correspondingly in the brain of the 60 day old mice. During the next two months the decrease becomes 20% per month, and during the following 8 months, about 12–15% per month. After that it becomes less than 10% per month. In total, the number of proliferating cells in the SGZ decreases 64 fold from 4500 to 70 and the local cell density decreases 38 fold from 67 to 1.8 (Table 1, Fig. 3).

The SGZ spans 4 mm along the dorso-ventral axis in the mouse brain. The majority of proliferating cells are located in the dorsal part of SGZ where they also have a higher cell density (Fig. 4A, D). Their number and density steadily decreases toward the ventral part of the SGZ with very few proliferating cells in the most ventral part of SGZ, even in the brain of the 30 day old mice (Fig. 4A, D). We do not find any part of the SGZ along the dorso-ventral axis where the number or density of proliferating cells is maintained with age. It appears that the number and density of proliferating cells decrease in all parts of SGZ with age (Fig. 4A, D). To confirm this observation, we divided the SGZ into four equal 1 mm thick slices along the dorso-ventral axis. The most

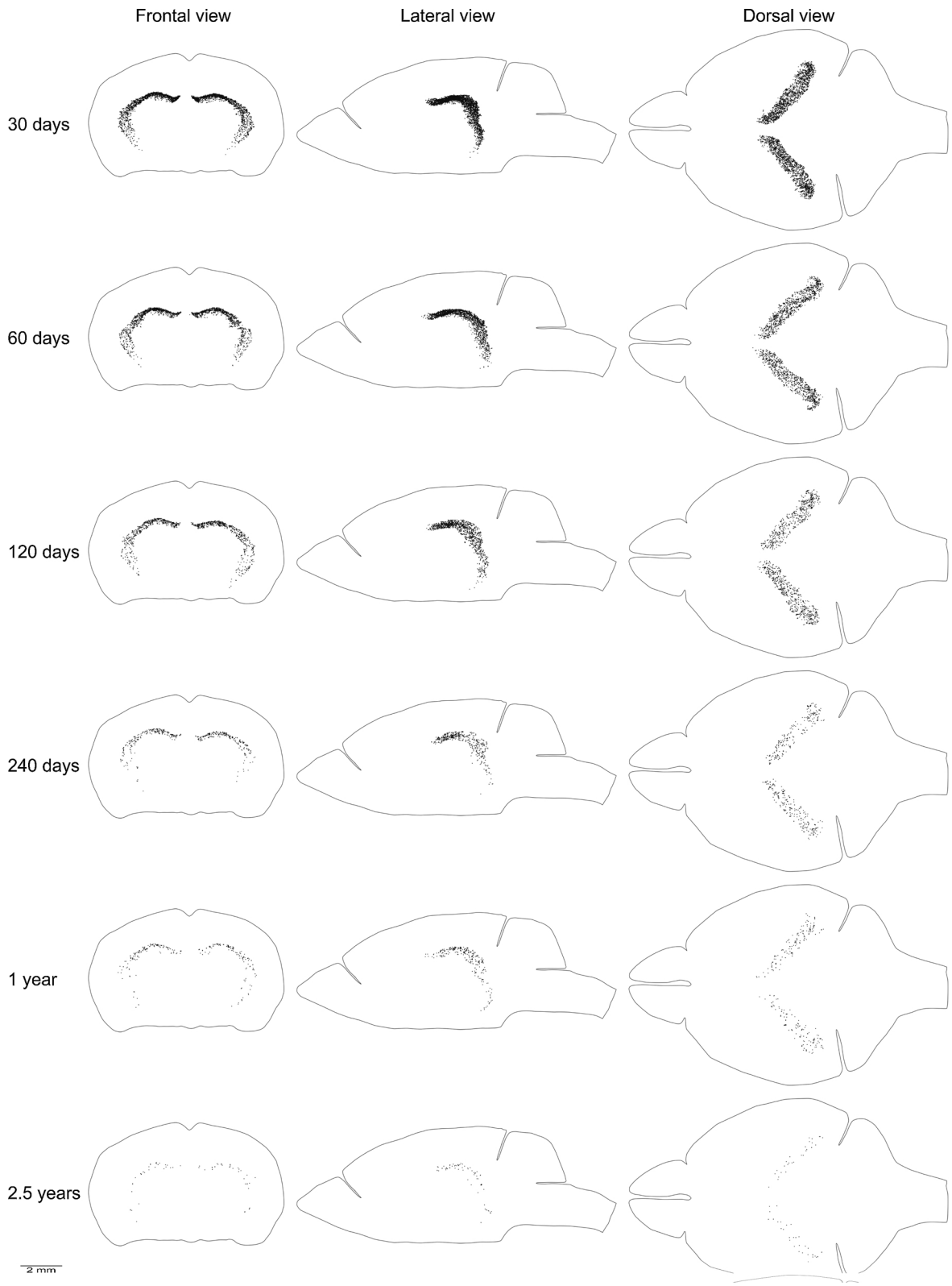

Fig. 2. Distribution of proliferating cells in the SGZ.
Each EdU-labelled nucleus located in the SGZ is shown as a black dot. The brain shape is outlined with a black line. Frontal, lateral, and dorsal views of the brain are shown. Mouse age is shown on the left.

dorsal slice contains 77% of all proliferating cells in the SGZ in 30 day old mice. The next slices contain 13%, 8% and 2% correspondingly (Fig. 5A). The average proliferating cell density also is highest in the most dorsal slice of SGZ and decreases in the more ventral slices from 79 to 32, 20 and 9 correspondingly (Fig. 5B). Despite the significant difference in the number and density of proliferating cells in different SGZ slices, the rate of their decrease with age is very similar in all SGZ slices (Fig. 5C, D).

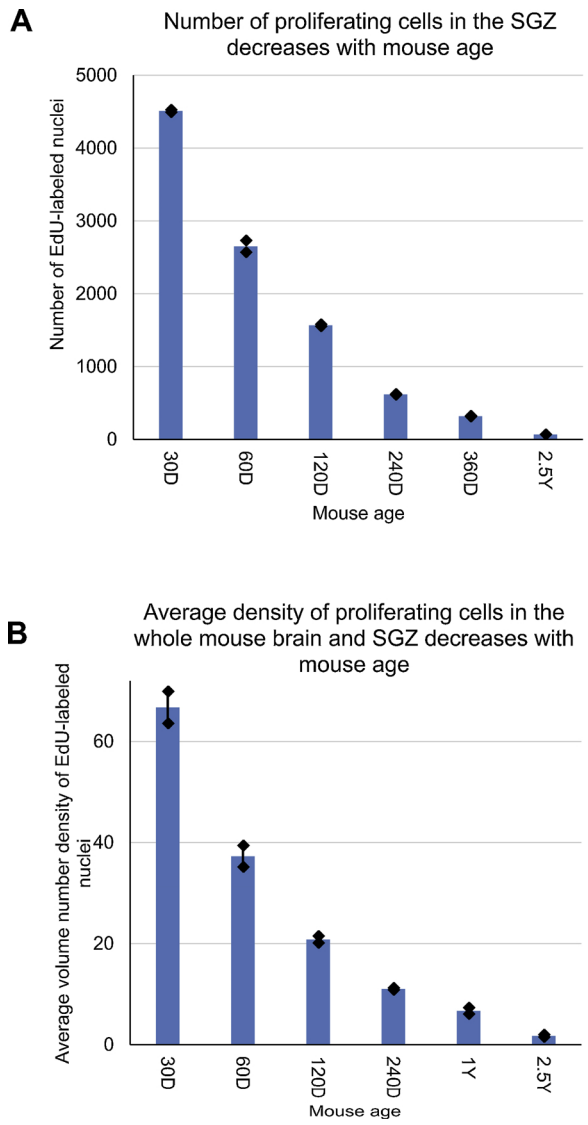

Fig. 3. Age-related decrease in the number and average density of proliferating cells located in the whole mouse brain and the SGZ.
(**A**). The number of proliferating cells in the SGZ decreases with mouse age. The means are significantly heterogeneous (one-way ANOVA, $F_{5,\ 6} = 2459$, P = 7.61E-10). The post-hoc *t*-test shows that all means are significantly different from each other ($P < 0.05$). (**B**). The average density of proliferating cells in the SGZ decreases with mouse age. The average volume number density is calculated as the average number of neighbouring EdU-labelled nuclei located closer than 200 μm to each EdU-labelled nucleus. The means are significantly heterogeneous (one-way ANOVA, $F_{5,\ 6} = 230$, P = 9.08E-7). The post-hoc *t*-test shows that all means are significantly different from each other ($P < 0.05$). Error bars show standard deviation.

SGZ spans 3 mm along the antero-posterior axis (Fig. 4B, E). Proliferating cells are distributed more evenly along this axis. We also observed that the number and density of proliferating cells decrease in all parts of the SGZ along this axis with the age increase (Fig. 4B, E). The mouse brain contains two SGZs. One is located on the left side of the brain and the other on the right side. Each SGZ spans 3 mm along the left-right axis with a small gap between them in the middle of the brain (Fig. 4C, F). Proliferating cells are distributed relatively evenly along the left-right axis with the higher volume number density toward the middle of the brain (Fig. 4C, F). The number and density of proliferating cells decrease in all parts of SGZ along this axis relative to the age increase similar to what we observe along the dorso-ventral axis.

The SGZ is a thin cellular layer on the inner surface of the granule cell layer in the dentate gyrus (DG) and is essentially a planar structure. The SGZ has a wedge-like shape (Fig. 6A), and we can distinguish an external arm of the SGZ that underlines the external arm of the granule cell layer that faces the cortex. There is also an internal arm that underlines the internal arm of the granule cell layer that faces the mesencephalon or diencephalon (Altman and Das, 1966). The tip of the wedge can be identified as the apex of the DG hilus (Fig. 6A). We virtually transformed the distribution of proliferating cells in the SGZ of 60 day old mouse and represented it as a flat surface with traces of the hilus apex as a line that divides the flattened internal and external arms of the SGZ (Fig. 6B). The approximate shape of the internal and external SGZ arms were obtained by tracing the margins of both arms. The distribution of proliferating cells on the flattened SGZ appears to be random with no apparent empty spaces. Some aggregation of proliferating cells could be seen, but the aggregating appears in different parts of SGZ on the left and right side of the brain showing that no apparent pattern exists in their distribution. The ventrolateral end of the SGZ has a significantly lower density of proliferating cells than the dorsomedial end and the medial part (Figs. 6B, 7 A). This trend can be observed in the internal and external SGZ arms (Figs. 6B, 7 B, C). By smoothing the graphs showing the distribution of proliferating cells along the apex of the DG hilus (Fig. 7A), we found that the highest number of proliferating cells are located approximately 0.75 mm from the dorsomedial end of the SGZ (Fig. 7D) which corresponds to the most dorsal part of the DG.

The distribution of proliferating cells across the SGZ shows that the highest number of proliferating cells is located near the hilus apex mostly on the external SGZ arm (Fig. 7E). This peak is surrounded by shoulders with a fairly even distribution of proliferating cells that extend in both arms 0.4 mm from the hilus apex. The steady decline of the number of proliferating cells is observed beyond the shoulders (Fig. 7E). The steep decline in the number of proliferating cells can be observed at the position of the hilus apex (Fig. 7E). This decline is observed because the proliferating cells in this part of SGZ are located at some distance from the granule cell layer in contrast to other parts of SGZ where they are located immediately on the surface of the granule cell layer. The distribution across SGZ also shows that the number of proliferating cells located in the external arm is larger than that in the internal arm (Fig. 7E, F).

The local density of proliferating cells varies greatly in the SGZ of 30 day old mice from 180 to 1 (Fig. 8A). The distribution shows a steady increase in the number of proliferating cells with the local density increasing from 1 to 30. The number of proliferating cells with local cell densities from 30 to 110 remains fairly constant, and after that it steadily declines (Fig. 8A). The distribution does not show any peaks or other irregularities that could indicate the presence of two or more separate populations of proliferating cells in the SGZ. The distribution in the brains of 60 day old mice resembles the distribution in 30 day old mice, but with the highest density about 100. The distribution in older mice continues to show single-peak with the progressive decrease of the highest density with age (Fig. 8A). The highest density reaches only 5 in the 2.5 year old mice which is 36 times less than in 30 day old mice.

Proliferating cells in the SGZ could be randomly distributed, or they could form clusters where dense groups of proliferating cells are surrounded by the areas without proliferating cells. To evaluate these two possibilities, we calculated a ratio for each proliferating cell between the number of other proliferating cells located closer than 50 μm and the number of proliferating cells located closer than 200 μm. If cells are distributed randomly one would expect that in a planar structure the number of proliferating cells located closer than 50 μm be 16 fold smaller than the number of cells located closer than 200 μm. This is because the area of the circle with a 50 μm radius is 16 times smaller than the circle with a 200 μm radius. On the other hand, one could expect this ratio to be 1/64 for proliferating cells distributed randomly in the volume because the volume of the sphere with a 50 μm radius is 64 times smaller than with a 200 μm radius. Any deviation of the ratio

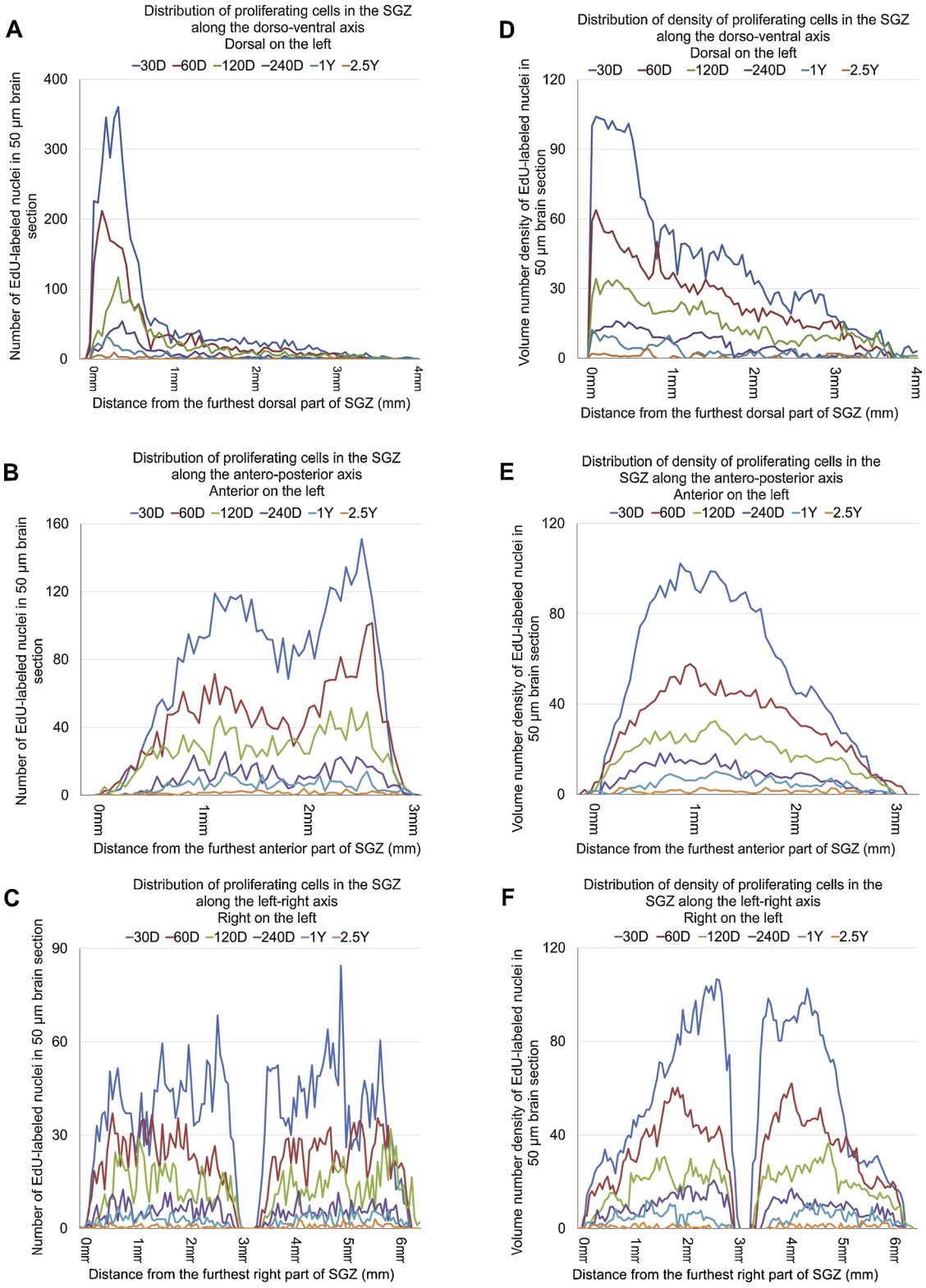

Fig. 4. Distribution of proliferating cells in the SGZ along the dorso-ventral, antero-posterior, and left-right axis in a mouse brain.
(**A**, **B**, **C**). Distribution of proliferating cells. The number of EdU-labeled nuclei in a 50 µm brain section is shown along the vertical axis of the charts. (**D**, **E**, **F**). Distribution of average volume number density of proliferating cells. The average number of neighboring EdU-labeled nuclei located closer than 200 µm to each EdU-labeled nucleus in a 50 µm brain section is shown along the vertical axis of the charts. (**A**, **D**). Distribution along the dorso-ventral axis. The distance from the furthest dorsal part of the SGZ is shown along the horizontal axis of the charts. (**B**, **E**). Distribution along the antero-posterior axis. The distance from the furthest anterior part of the SGZ is shown along the horizontal axis of the charts. (**C**, **F**). Distribution along the left-right axis. The distance from the furthest right part of the SGZ is shown along the horizontal axis of the charts.

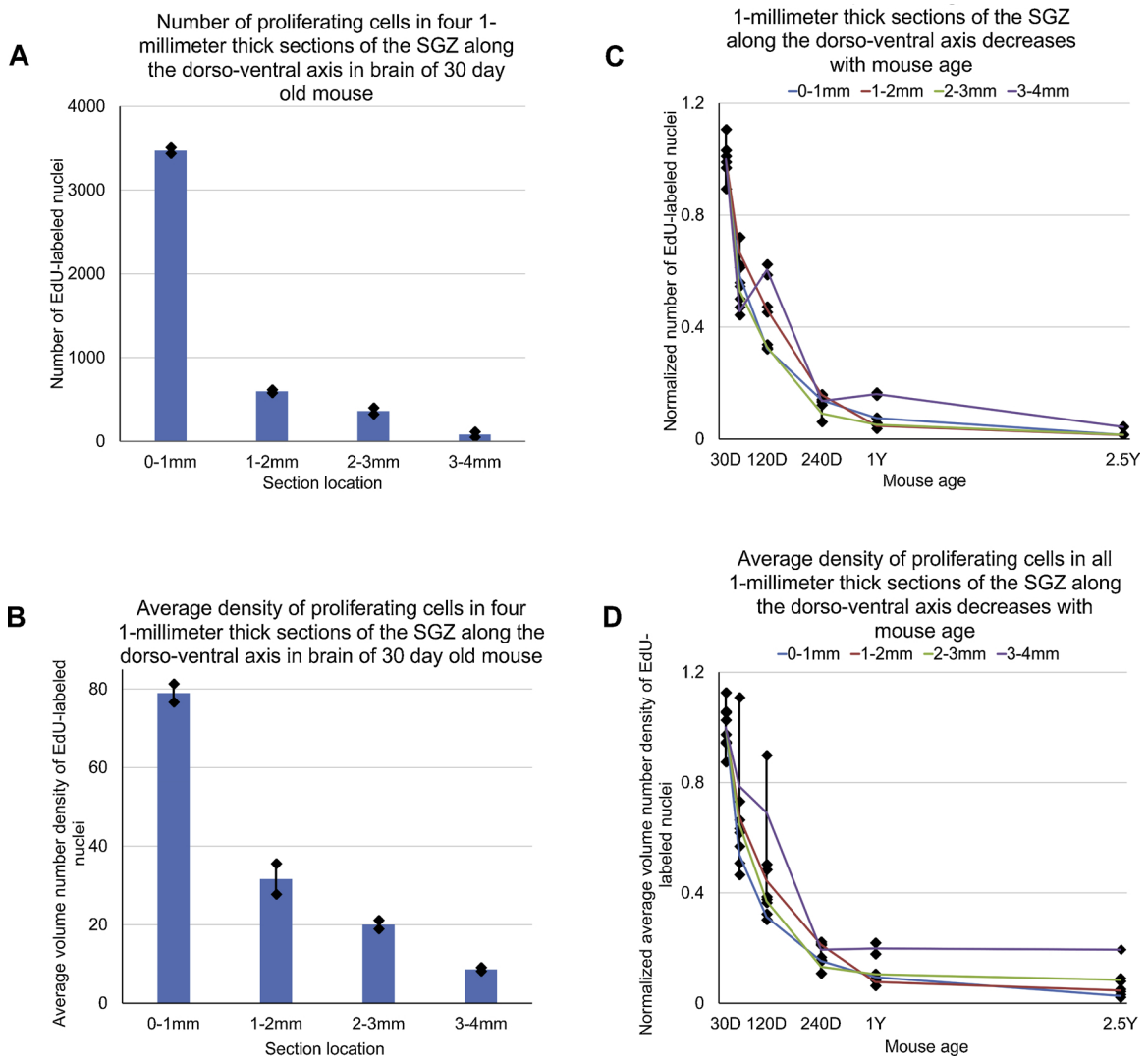

Fig. 5. The number and average density of proliferating cells in four 1-millimeter thick sections of the SGZ along the dorso-ventral axis decreases with mouse age. (**A**). The number of EdU-labelled nuclei in four 1-millimeter thick sections of the SGZ along the dorso-ventral axis in the brain of a 30 day old mouse. The section position is shown along the horizontal axis of the charts. The means are significantly heterogeneous (one-way ANOVA, $F_{3,\ 4} = 2418$, $P = 5.69E\text{-}7$). The post-hoc *t*-test shows that all means are significantly different from each other ($P < 0.05$). (**B**). The average volume number density of EdU-labelled nuclei in four 1-millimeter thick sections of the SGZ along the dorso-ventral axis in brain of a 30 day old mouse. The section position is shown along the horizontal axis of the charts. The means are significantly heterogeneous (one-way ANOVA, $F_{3,\ 4} = 171$, $P = 1.12E\text{-}4$). The post-hoc *t*-test shows that all means are significantly different from each other ($P < 0.05$) except the mean for the 1–2 mm section and the 2–3 mm section ($P = 0.10$). (**C**). The number of EdU-labelled nuclei in all 1-millimeter thick sections of the SGZ along the dorso-ventral axis decreases with mouse age. The number of EdU-labelled nuclei in each section is normalized to the number of EdU-labelled nuclei in the same section in the brain of a 30 day old mouse. (**D**). The average volume number density of EdU-labelled nuclei in all 1-millimeter thick sections of the SGZ along the dorso-ventral axis decreases with mouse age. The average volume number density of EdU-labelled nuclei in each section is normalized to the average volume number density of EdU-labelled nuclei in the same section of the brain of a 30 day old mouse. Error bars show standard deviation. The distance is measured from the furthest dorsal part of the SGZ.

from 1/16 or 1/64 should indicate that proliferating cells are distributed in a non-random manner. The distribution of proliferating cells in the SGZ follows the 1/16 line as expected for randomly distributed cells in a planar structure for proliferating cells with the local number cell density from 1 to 40 (Fig. 8B). This ratio is lower for proliferating cells with the higher cell density (Fig. 8B).

The distribution of the ratio appears to be slightly above 1/16 line at cell densities between 1 and 20 (Fig. 8B). This might indicate that a fraction of the proliferating cells in the SGZ is located in small clusters. We calculated the fraction of proliferating cells that have 1, 2, 3, 4, or 5 proliferating neighbours located closer than 10 μm and found that two thirds of the proliferating cells have no close neighbours, 25% of them have one other proliferating cell located closer than 10 μm, 6% have two neighbours and 1% have three (Fig. 8C). These numbers are very close for 30, 60, 120 and 240 day old mice, somewhat lower in the 1 year old mice and even lower in the 2.5 year old (Fig. 8C).

Discussion

The labelling of proliferating cells with Bromodeoxyuridine (BrdU) or EdU (Chehrehasa et al., 2009; Zeng et al., 2010; Benjamin et al., 2017) is a commonly used technique. These thymidine analogs are able to incorporate into replicating chromosomal DNA during the S phase of the cell cycle which allows detection of all proliferating cells. The length of the S phase of the cell cycle in neural precursors does not appears to change with age (Olariu et al., 2007) thereby allowing to obtain a consistent measurement of neural precursor production using BrdU or EdU at different ages. The neural stem and progenitor cells

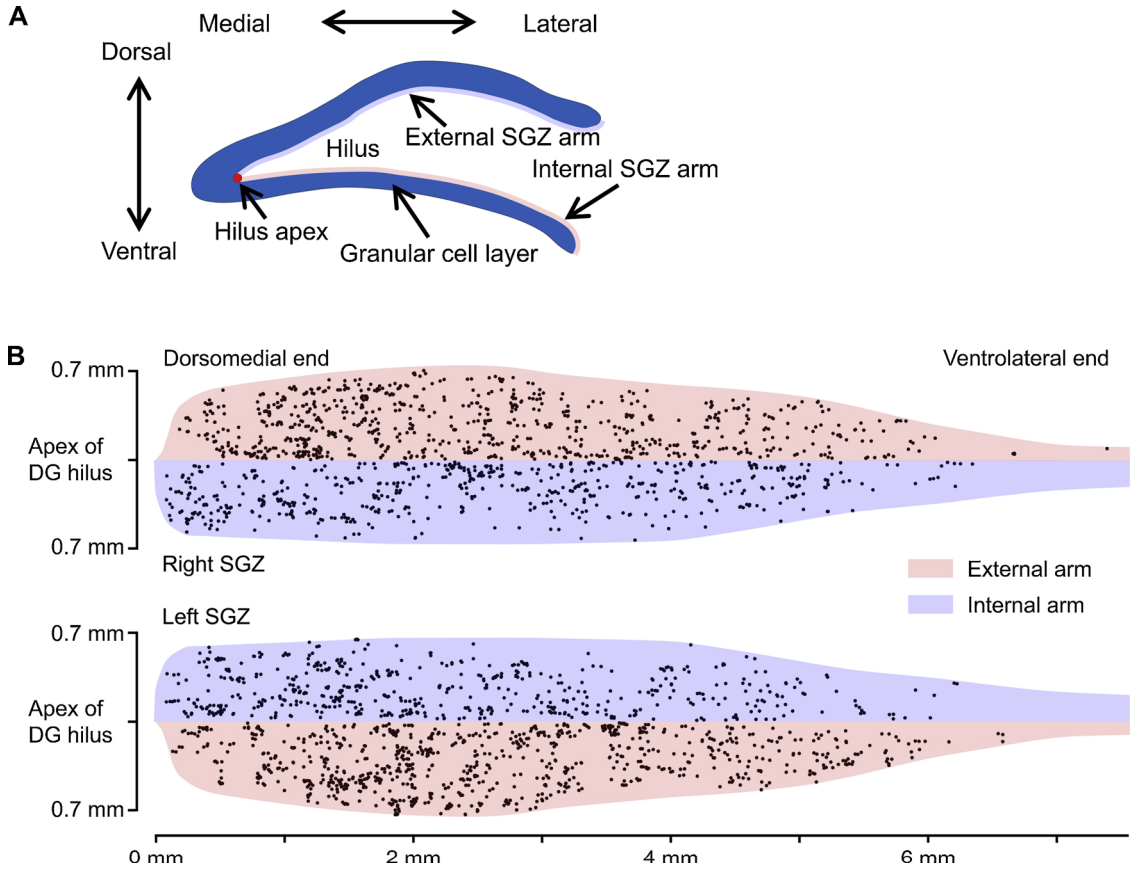

Fig. 6. Distribution of proliferating cells in the flattened SGZ of a 60 day old mouse.
(**A**). Schematic drawing of a coronal section of the dorsal part of DG showing the location of the external and internal SGZ arms and the apex of DG hilus. (**B**). Distribution of proliferating cells in the flattened SGZ of a 60 day old mouse. The line that traces the apex of DG hilus was established for the left and right DG in the 3D reconstruction of a 60 day old mouse brain, and the perpendicular (shortest) distances from this line to all EdU labelled cell nuclei in the SGZ was calculated using the line and nuclei coordinates. To generate the flattened image, we straightened the apex lines and showed EdU labelled nuclei as black dots according to the position of these nuclei along the apex lines and the distance from the apex lines. EdU labelled nuclei located in the internal and external arms of the SGZ are shown on different sides of straightened apex lines as indicated in the figure. The distance from the dorsomedial end of the SGZ is shown at the bottom. The distance from the apex lines is shown on the left.

account for 98% of all dividing cells in the SGZ in the mouse brain (Fig. 1f in (Encinas et al., 2011)) and a majority of them differentiate into new neurons (Brown et al., 2003; Snyder et al., 2009a). Therefore, in this study, we have not used any additional markers to distinguish neural progenitor cells from any other proliferating cells in the SGZ.

Cells labelled with BrdU or EdU continue to divide and produce progeny that are also labelled (Encinas et al., 2011). Therefore, for an accurate measurement of the rate of cell proliferation in the SGZ, the labelling time should be sufficiently short to prevent division of these labelled cells. We used a 1 h labelling time in this study because an extension of labelling time to 2 h leads to the appearance of divided labelled cells in the mouse brain (Bordiuk et al., 2014). This is in contrast to many publications that use either a 2 h labelling time or even a longer multiday and multi-injection labelling protocol to address cell proliferation in the SGZ (van Praag et al., 1999; Tapia-González et al., 2013) and makes it rather impossible to directly compare results obtained in these studies and our study.

We examined publications using a single injection of BrdU and found that the number of proliferating cells found in the SGZ varied greatly. Walker et al. found 2100 labelled nuclei in the SGZ of 8 week old mice after 2 h labelling (Walker et al., 2013); DeCarolis et al. found 3200 labelled nuclei in the SGZ of 9–14 week old mice after 24 h labelling (DeCarolis et al., 2014); Walter et al. found 1025 labelled nuclei in the SGZ of 3 month old mice after 2 h labelling (Walter et al., 2011); Tapia-González et al. found 734 labelled nuclei in the SGZ of 3–4 month old mice after 30 min labelling (Tapia-González et al., 2013); Sui et al. found 260 labelled nuclei in the SGZ of 16–20 week old mice after 2 h labelling (Sui et al., 2013); and Contet et al. found 2500 labelled nuclei in the SGZ of 4–6 month old mice after 2 h labelling. We list results in the order of mouse age increase and expect that with the age increase the number of proliferating cells counted in the SGZ will decrease. To our surprise the numbers increase and decrease in what appears to be a random manner. The difference could reach almost ten times in mice of similar age showing that differences in labelling and counting protocols could result in the detection of profoundly different numbers of proliferating cells in the SGZ.

One notable feature of the majority of the above-mentioned studies is the use of mice of no particular age but rather within the age interval such as 4–6 month old or 9–14 week old. It is notable because the difference between the number of proliferating cells in the youngest and the oldest mice in these groups could reach 30%. Just using mice in one experimental group comprising mostly from younger mice and in another mostly from older mice could be result in a difference of 20%–30% between these experimental groups even if experimental conditions have no effect on cells proliferation in the SGZ. On the basis of our data we could calculate the difference in cells proliferation in the SGZ that one day makes. This difference is about 2% between age of 30 and 60 days; about 1% between age of 60 and 120 days; about 0.8% between age of 120 and 240 days; about 0.6% between age of 240 days and 1 year; and about 0.35% between age of 1 and 2.5 years. Thus, mice in any experiment studying neurogenesis in the SGZ should be exactly the same age or as close as possible and in the former case the

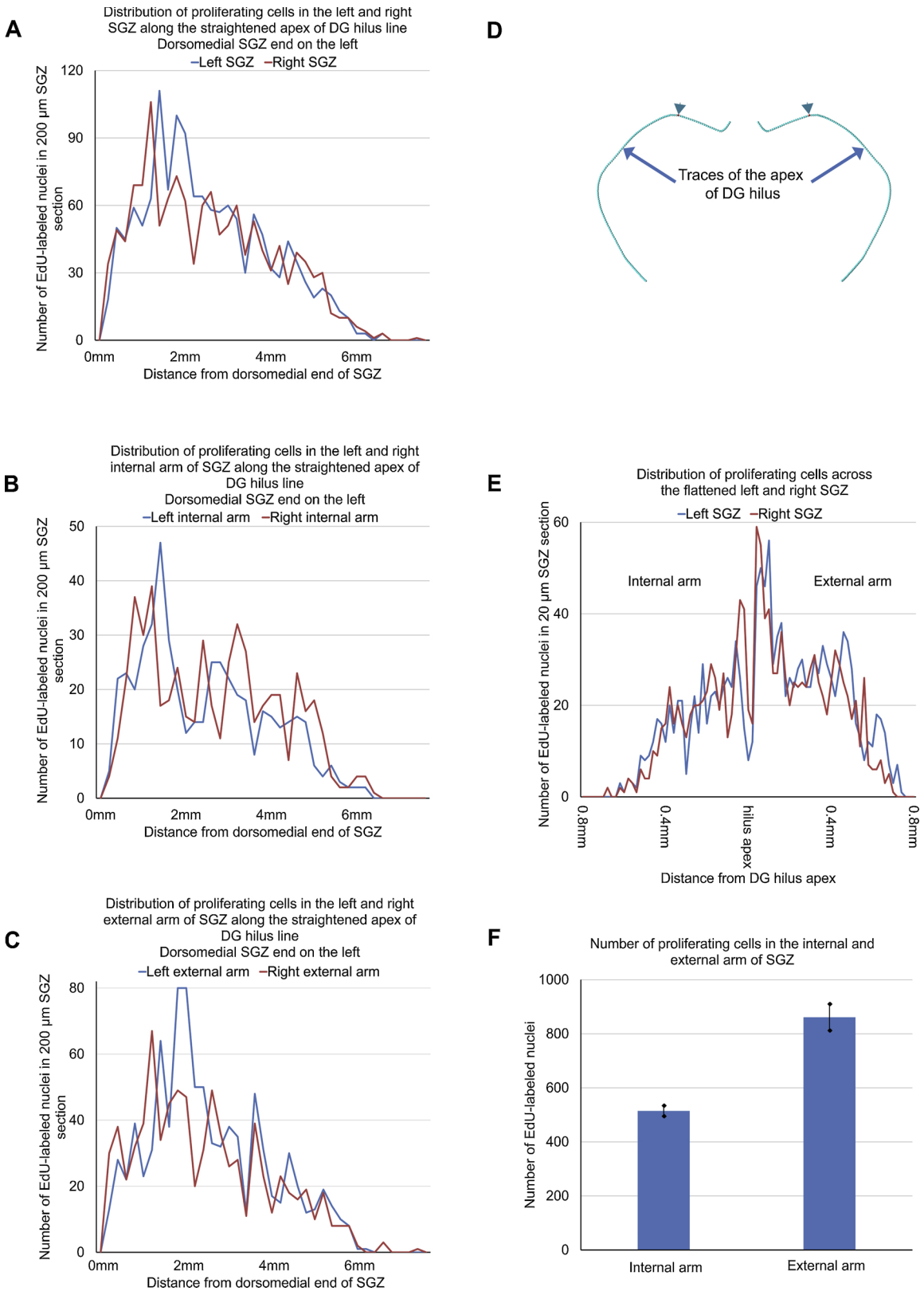

Fig. 7. Distribution of proliferating cells along and across the flattened SGZ of a 60 day old mouse.
(**A**). Distribution of EdU labelled nuclei in the left and right SGZ along the straightened apex of the DG hilus line. (**B**). Distribution of EdU labelled nuclei in the left and right internal arm of SGZ along the straightened apex of the DG hilus line. (**C**). Distribution of EdU labelled nuclei in the left and right external arm of the SGZ along the straightened apex of DG hilus line. (**D**). Location of the highest number of proliferating cells in the SGZ is shown by arrowheads along traces of the apex of the DG hilus. Coronal view. (*E*). Distribution of EdU labelled nuclei across the flattened left and right SGZ. (**F**). Number of EdU labelled nuclei in the internal and external arm of SGZ. Error bars show standard deviation. The *t*-test shows that means are significantly different from each other ($P < 0.05$).

experimental groups should be balanced for the mouse age. In our experiment we use mice born on the same day in all experimental groups but 2.5 year group. The 2.5 year old mice were obtained from the aged mice collection of the Institute of aging (NIH) that provides only the month of mice birth.

One of our goals was to study the spatial distribution of proliferating cells in the SGZ. Consequently, we could not use stereological methods for section analysis, as stereology does not provide spatial information. It can be only used to estimate the number of proliferating cells in the SGZ. Therefore, we opted out for the use of point cloud approach (Bordiuk et al., 2014). In this approach we directly count all EdU stained nuclei in the SGZ and obtain their coordinates on all sections in each analysed mouse brain. Counting all proliferating cells in the SGZ on mouse brain sections was done before for Ki67 (Ben Abdallah et al., 2010; Amrein et al., 2015) and BrdU staining (DeCarolis et al., 2014). The major concern about such counting is a possibility that some nuclei of proliferating cells could be cut across during section preparation and their fragments will be present on two consecutive sections. Consequently, counting all stained nuclei on these sections should lead to the counting of each fragment as positive nucleus that may lead to the overestimation of proliferating cells number in the SGZ. We tested this assumption by counting EdU stained nuclei located at the same position on two consecutive brain sections. We estimated that around 10% of all EdU stained nuclei should be cut during section preparation based on the assumption that nuclei of proliferating cell in the SGZ is about 5 μm in diameter. However, we found only 4 probable pairs of EdU stained nuclei among 617 counted. Thus, the majority of cut nuclei fragments are likely lost and direct counting should lead to the undercount of proliferating cells in the SGZ. This undercount could reach 10% if during section preparation all fragments of cut nuclei are lost.

We found that the numbers of proliferating cells obtained by direct counting of all proliferating cells in the SGZ on all brain sections are consistent in mice of the same age (Fig. 3A), and despite a small sample size (n = 2), a one-way ANOVA shows that the measurements we obtained for mice at different ages are significantly heterogeneous (P = 7.61E-10). In addition, the post hoc *t*-test shows that all measurements are significantly different from each other ($P < 0.05$). Originally, the Student's *t*-test was developed using sample size n = 4 (Student, 1908). Recently it was shown that the Student's *t*-test could be reliably used for sample size n = 2 especially for cases with the effect size D bigger that 10 Cohen units (de Winter, 2013). The smallest effect size in our study between two experimental groups is 13.2. We also used the Tukey HSD as an alternative post hoc test and found again that all measurements are significantly different from each other (x-crit = 193.4).

The decrease of hippocampal neurogenesis in rats with age was noticed by Dr. Joseph Altman in 1965 (Altman and Das, 1965). Later this decrease was reported in many other mammalian species (Seki and Arai, 1995; Kuhn et al., 1996; Drapeau and Nora Abrous, 2008; Morgenstern et al., 2008; Lee et al., 2012; Apple et al., 2017; Mosher and Schaffer, 2017; Smith et al., 2017). Despite many reports of the decline of neurogenesis with age, there is no published detailed analysis of the age effect on neurogenesis in the SGZ in mice (Table 1 in (Drapeau and Nora Abrous, 2008)) similar to what is presented in our study. The cell proliferation decline in the SGZ with age which we are reporting in this study is similar to the reported decline of the number of BrdU labelled cells (Bondolfi et al., 2004), Ki67 (Ben Abdallah et al., 2010; Gil-Mohapel et al., 2013), PCNA (Gil-Mohapel et al., 2013) and DCX (Ben Abdallah et al., 2010) expressing cell in the SGZ. Despite the similarity in the extent of the reported decrease, the numbers of proliferating cells reported in these studies are substantially different from what we are reporting in our study. This is due to use 5-day labelling protocol in the study with BrdU labelling (Bondolfi et al., 2004) and the difference in the length of S phase of the cell cycle and periods when Ki67, PCNA, and DCX are expressed in proliferating neural progenitors.

The decline of cell proliferation in the SGZ continues during the entire mouse life. We have not noticed periods in the mouse life when cell proliferation continues at a steady rate (Fig. 3). The continued decrease is observed in areas with high and low density of proliferating cells (Figs. 4 and 5). A visualisation of the distribution of proliferating cells (Fig. 2) does not reveal any local areas in the SGZ where cell proliferation is maintained for a considerable period of time at the similar level. The steady state cell production is the hallmark of cell renewal in skin, intestinal epithelia and blood. Such stable and continued cell production balances the continued and stable loss of worn-out cells

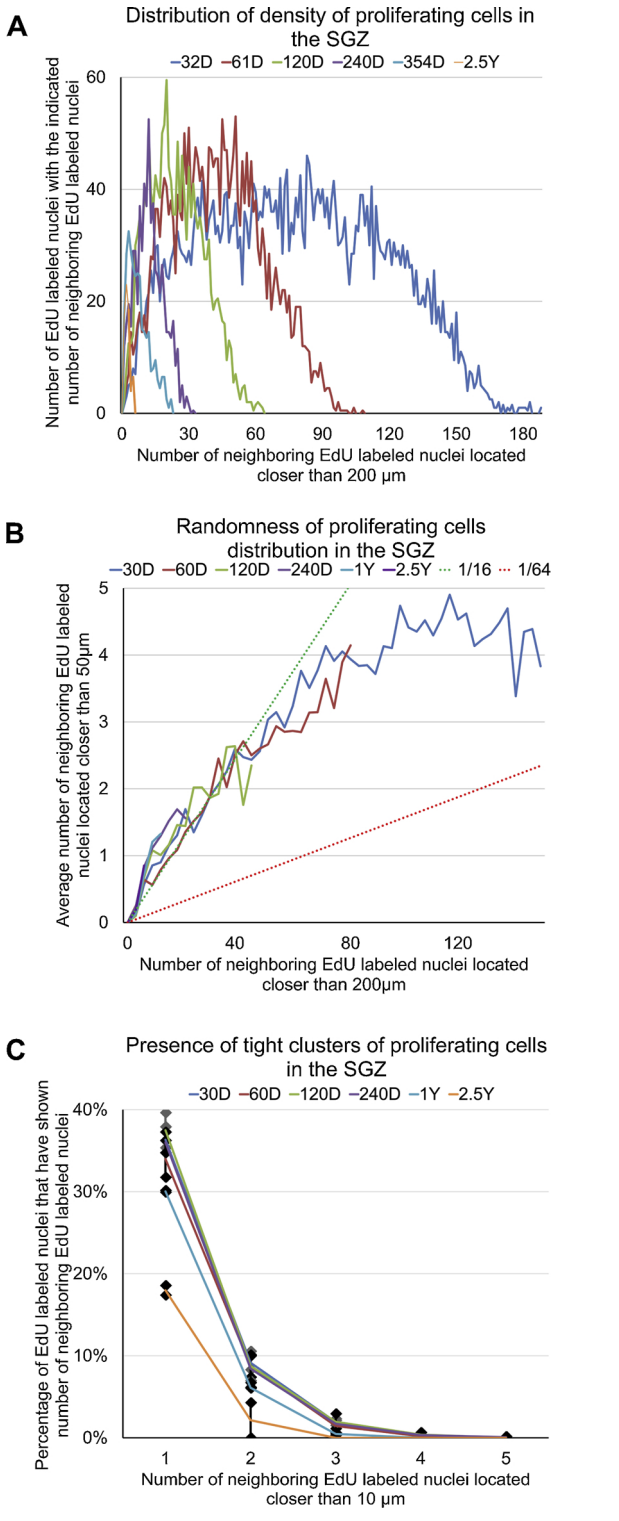

(caption on next page)

Fig. 8. Characterization of proliferating cells distribution in the SGZ.
(**A**). Distribution of volume number density of proliferating cells in the SGZ. The number of neighbouring EdU labelled nuclei located closer than 200 μm is shown along the horizontal axis of the chart. The number of EdU labelled nuclei with the indicated number of neighbouring EdU labelled nuclei is shown along the vertical axis. (**B**). Randomness of proliferating cells distribution in the SGZ. The number of neighbouring EdU labelled nuclei located closer than 200 μm is shown along the horizontal axis of the chart. The average number of EdU labelled nuclei located closed than 50 μm to each EdU labelled nuclei with the same number of neighbouring EdU labelled nuclei located closer than 200 μm is shown along the vertical axis of the chart. The graph also shows 1/16 and 1/64 lines. (**C**). Presence of tight clusters of proliferating cells in the SGZ. The number of neighbouring EdU labelled nuclei located closer than 10 μm is shown along the horizontal axis of the chart. Percentage of EdU labelled nuclei that have the indicated number of neighbouring EdU labelled nuclei is shown along the vertical axis of the chart. Error bars show standard deviation.

in these tissues and maintains them in a homeostasis. The continued decrease of cells proliferation in the SGZ shows that the processes these new cells are intended to support do not require the steady supply of new neural progenitors or that this process is not homeostatic.

EdU is incorporated into chromosomal DNA only during the S phase of the cell cycle. The length of the S phase in neural precursors in the SGZ is approximately 7.6 h (Hayes and Nowakowski, 2002). Based on this number and our data about cell proliferation in the SGZ, we can calculate that from the age of 30 days to the age of 2.5 years 1.51 million new cells are produced in the SGZ if we assume that the number of proliferating cells in the SGZ decreases exponentially between measured points. The number becomes 1.60 million if we assume that the decrease is linear. Cell production changes considerably during mouse life. Thus, about 350,000 new cells are produced in the SGZ during the 30 days between ages of 30 and 60 days. In contrast, it takes 1.5 years to produce the same number of new cells toward the end of mouse life between ages of 260 days and 2.5 years. The number of granule cells in mouse hippocampus is about 500,000 (Kempermann et al., 1997a; Farrar et al., 2005; Ben Abdallah et al., 2010; Tapia-González et al., 2013). Given this, all granule cells could be replaced by new cells three times during the lifespan of the mouse. However, only a small fraction of granule cells are replaced because only some of the neural precursors differentiate into new neurons, and the majority of new neurons undergo programmed cell death (PCD) during processes of differentiation and integration into the granule cell layer (Biebl et al., 2000). The rate of cell proliferation in the SGZ in C27BL/6 J mice appears to be almost twice as high as in other commonly used mouse strains (Kempermann et al., 1997b). This rate is also sensitive to housing conditions and access to exercise equipment (Kempermann et al., 1997a; van Praag et al., 1999). Therefore, neural precursor production in other mouse strains or mice hosted in different conditions could be different than reported in our study.

Our estimate of the production of new cells in the SGZ is vastly larger than the estimate presented in the recent publication by Pilz et al. (2018). Using chronic live imaging of neurogenesis in the SGZ in two month old mice, the authors estimated that only 45,000 new cells are produced in the SGZ during the entire mouse lifespan. For comparison, this number of new cells represents only 3% of our estimate and such a number of new cells in the SGZ should be produced in less than six days in two month old mice according to our data. The simplest explanation for this apparent discrepancy could be that the removal of the neocortex above the hippocampus, required for the direct neurogenesis observation, causes brain trauma which suppresses proliferation of RGL cells in the SGZ. Another plausible explanation is that the RGL cell labelling method relying on the activity of Achaete-scute homolog 1 (Ascl1) promoter selectively labels RGL cells with low proliferative potential. In this case we should expect that other RGL cells, that are not labelled by this method, have high proliferative potential and are responsible for the production of 97% new cells in the SGZ. We might also expect that 97% of new cells in the SGZ are produced by non-RGL cells or that such cells produce new RGL cells that, in turn, produce new neuronal precursors in the SGZ. All these possibilities need to be tested experimentally. The utility of our estimate is that we provide the total number of new cells produced in the SGZ. Thus, the comparison of this number with the number of new cells produced by some particular RGL or other cells in the SGZ, as we show above, will immediately reveal the relative contribution of such cells in neurogenesis in the SGZ.

Several experimental approaches have previously been used to study neurogenesis in different parts of the SGZ. One of them is to divide the SGZ along the anteroposterior axis of the mouse brain on the rostral SGZ and caudal SGZ (Olariu et al., 2007; Kanatsou et al., 2017). Another is to divide SGZ along dorsoventral axis (Banasr et al., 2006; Snyder et al., 2009b; Jinno, 2011; Nollet et al., 2012; Tanti et al., 2012); to study neurogenesis in the external and internal SGZ arms (Fig. 6A) (Kempermann et al., 2003; Olariu et al., 2007; Snyder et al., 2009b; Jinno, 2011; Kanatsou et al., 2017); or to use isolated and straightened hippocampi and divide it longitudinally (Wiget et al., 2017). In our study, we obtained coordinates of all proliferating cells in the SGZ and represented them as a point cloud. Using this approach it is possible to visualize the distribution of proliferating cells in the SGZ at different mouse ages (Fig. 2), show the distribution of the number and density of proliferating cells along dorso-ventral and other axis of the SGZ (Fig. 4), evaluate the randomness of distribution and clustering of proliferating cells in the SGZ (Fig. 8), and flatten the SGZ to evaluate distribution of proliferating cells along the longitudinal axis and across of the SGZ (Figs. 6 and 7). All these used in our study analyses allow a detailed characterization of proliferating cell distribution in the SGZ to better understand how their distribution changes with age. In contrast, the above mentioned approaches, with the exception of Wiget at al. study (Wiget et al., 2017), provide only a number of proliferating cells in some particular part(s) of the SGZ.

The distribution of proliferating cells shows no periodicity, expansive empty spaces or abrupt changes along the SGZ (Figs. 2,4–7). We found that proliferating cells are distributed throughout the entire SGZ at all analysed ages (Figs. 2,4 and 5). This finding shows that the zone of proliferation in the SGZ does not shrink with increased age, but rather the rate of cell proliferation decreases in all parts of the SGZ (Fig. 5). The ratio between the number of proliferating cells located closer than 200 μm to the number located closer than 50 μm clearly shows that proliferating cells in the SGZ have a planar distribution (Fig. 8B). We show that this ratio becomes smaller than 1/16 for proliferating cells with a high local density (Fig. 8B). Proliferating cells in the SGZ areas with a high density are located not only on the inner surface of the granule cell layer but also small distances into the hilus; which makes their distribution more like a three-dimensional distribution.

The dorsal hippocampus appears to be mostly involved in cognitive functions such as spatial learning and memory and the ventral hippocampus in emotional reactions. And, correspondingly it was speculated that neurogenesis in the dorsal part of the SGZ affects cognitive functions and in the lateral part emotional functions such as stress or depression (reviewed in (Moser and Moser, 1998; Sahay and Hen, 2007; Fanselow and Dong, 2010; O'Leary and Cryan, 2014; Wu et al., 2015)). The majority of proliferating cells are located in the dorsal part of the SGZ (Fig. 4A, 5 A) mostly due to a higher density in the dorsal part of SGZ (Figs. 4B, 5 B). This trend continues during the mouse lifespan (Figs. 4A, D, 5). We have not found any evidence of an abrupt transition in the distribution of proliferating cells between the dorsal and ventral parts of the SGZ (Figs. 1, 2, 6B and 7 A) This could be explained by a possibility that functional difference of the dorsal and ventral DG is not reflected in the distribution of proliferating cells in the SGZ or that the boundary between dorsal and ventral parts of the DG is not abrupt. However, it is worthwhile to note that there is a profound difference in the number of proliferating cells between the dorsal and ventral parts of the SGZ. We found that the number of proliferating cells in the most

dorsal quarter of the SGZ is about 70-times higher than in the most ventral quarter (Fig. 5A).

We obtained the longitudinal distribution of proliferating cells in the SGZ by virtual transformation (Fig. 6B). This distribution looks very similar to the distribution observed in the straightened hippocampi (Fig.1A in (Wiget et al., 2017)) thereby showing validity of our approach. At the same time, our results, obtained by different experimental approach, confirm the finding by Wiget et al., (Wiget et al., 2017) that in C57BL/6 mice the highest rate of cell proliferation occurs about one third from the septal end of the SGZ that corresponds to the most dorsal part of the SGZ (Fig. 7D). The distribution of proliferating cells in DBA2/Crl, house and wood mice and bank voles are very different from C57BL/6 mice. The cell proliferation in these species/mouse strains are shifted toward the temporal part of the SGZ (Wiget et al., 2017) showing that even in closely related species/mouse strains the distribution of proliferating cells in the SGZ could be remarkably different. This difference shows that the higher rate of neural precursor production in the dorsal SGZ in C57BL/6 mice might not represent a typical distribution of neurogenesis in the SGZ. It also tempers hypotheses suggesting that neurogenesis plays a more significant role in cognitive/spatial functions of the hippocampus compared to emotional reactions.

The presence of neurogenesis in the SGZ in the adult human brain is still under discussion. Even in very recent publications, one may find data showing that neurogenesis stops completely at the age of 3 years (Dennis et al., 2016; Cipriani et al., 2018; Sorrells et al., 2018), and at the same time that neurogenesis is present at substantial levels even at a very old age (Spalding et al., 2013; Boldrini et al., 2018). One notable feature of adult neurogenesis studies in the human brain is that the human hippocampus is treated as a uniform structure. However, if one decides to study adult neurogenesis in the extreme ventral portion of the mouse hippocampus, there will be no detectable adult neurogenesis even in very young mice. Thus, in order to establish if a similar difference in the rate of neurogenesis between different parts of the human hippocampus also exists, the human SGZ needs to be analysed in a manner similar to our analysis of the mouse SGZ.

Conflict of interest

The authors declare no conflict of interest.

Acknowledgments

We thank R.E. Fine for providing comments and editing the manuscript, J.P. Morin, J.M. Wells, E. Hanlon and other members of New England Geriatric Research Education and Clinical Center for critical discussions; O. L. Bordiuk for technical assistance; N. Dziura for animal care. This study was supported by the Janet and Edward Gildea Charitable Foundation and is the result of work supported with resources and the use of facilities at the Edith Nourse Rogers Memorial Veterans Hospital, Bedford, Massachusetts, United States of America.

References

Aimone, J.B., Deng, W., Gage, F.H., 2011. Resolving new memories: a critical look at the dentate gyrus, adult neurogenesis, and pattern separation. Neuron 70, 589–596.
Altman, J., Das, G.D., 1965. Autoradiographic and histological evidence of postnatal hippocampal neurogenesis in rats. J. Comp. Neurol. 124, 319–335.
Altman, J., Das, G.D., 1966. Autoradiographic and histological studies of postnatal neurogenesis. I. A longitudinal investigation of the kinetics, migration and transformation of cells incorporating tritiated thymidine in neonate rats, with special reference to postnatal neurogenesis in some brain regions. J. Comp. Neurol. 126, 337–389.
Amrein, I., Nosswitz, M., Slomianka, L., van Dijk, R.M., Engler, S., Klaus, F., Raineteau, O., Azim, K., 2015. Septo-temporal distribution and lineage progression of hippocampal neurogenesis in a primate (Callithrix jacchus) in comparison to mice. Front. Neuroanat. 9, 85.
Apple, D.M., Solano-Fonseca, R., Kokovay, E., 2017. Neurogenesis in the aging brain. Biochem. Pharmacol. 141, 77–85.
Balu, D.T., Lucki, I., 2009. Adult hippocampal neurogenesis: regulation, functional implications, and contribution to disease pathology. Neurosci. Biobehav. Rev. 33, 232–252.
Banasr, M., Soumier, A., Hery, M., Mocaër, E., Daszuta, A., 2006. Agomelatine, a new antidepressant, induces regional changes in hippocampal neurogenesis. Biol. Psychiatry 59, 1087–1096.
Ben Abdallah, N.M.-B., Slomianka, L., Vyssotski, A.L., Lipp, H.-P., 2010. Early age-related changes in adult hippocampal neurogenesis in C57 mice. Neurobiol. Aging 31, 151–161.
Benjamin, J.S., Pilarowski, G.O., Carosso, G.A., Zhang, L., Huso, D.L., Goff, L.A., Vernon, H.J., Hansen, K.D., Bjornsson, H.T., 2017. A ketogenic diet rescues hippocampal memory defects in a mouse model of Kabuki syndrome. Proc. Natl. Acad. Sci. U. S. A. 114, 125–130.
Biebl, M., Cooper, C.M., Winkler, J., Kuhn, H.G., 2000. Analysis of neurogenesis and programmed cell death reveals a self-renewing capacity in the adult rat brain. Neurosci. Lett. 291, 17–20.
Boldrini, M., Fulmore, C.A., Tartt, A.N., Simeon, L.R., Pavlova, I., Poposka, V., Rosoklija, G.B., Stankov, A., Arango, V., Dwork, A.J., Hen, R., Mann, J.J., 2018. Human hippocampal neurogenesis persists throughout aging. Cell Stem Cell 22, 589–599 e5.
Bonaguidi, M.A., Wheeler, M.A., Shapiro, J.S., Stadel, R.P., Sun, G.J., Ming, G., Song, H., 2011. In vivo clonal analysis reveals self-renewing and multipotent adult neural stem cell characteristics. Cell 145, 1142–1155.
Bondolfi, L., Ermini, F., Long, J.M., Ingram, D.K., Jucker, M., 2004. Impact of age and caloric restriction on neurogenesis in the dentate gyrus of C57BL/6 mice. Neurobiol. Aging 25, 333–340.
Bordiuk, O.L., Smith, K., Morin, P.J., Semënov, M.V., 2014. Cell proliferation and neurogenesis in adult mouse brain. PLoS One 9, e111453.
Brown, J.P., Couillard-Després, S., Cooper-Kuhn, C.M., Winkler, J., Aigner, L., Kuhn, H.G., 2003. Transient expression of doublecortin during adult neurogenesis. J. Comp. Neurol. 467, 1–10.
Chehrehasa, F., Meedeniya, A.C.B., Dwyer, P., Abrahamsen, G., Mackay-Sim, A., 2009. EdU, a new thymidine analogue for labelling proliferating cells in the nervous system. J. Neurosci. Methods 177, 122–130.
Cipriani, S., Ferrer, I., Aronica, E., Kovacs, G.G., Verney, C., Nardelli, J., Khung, S., Delezoide, A.-L., Milenkovic, I., Rasika, S., Manivet, P., Benifla, J.-L., Deriot, N., Gressens, P., Adle-Biassette, H., 2018. Hippocampal radial glial subtypes and their neurogenic potential in human fetuses and healthy and alzheimer's disease adults. Cereb. Cortex 1991 (28), 2458–2478.
de Winter, J.C.F., 2013. Using the Student's t-test With Extremely Small Sample Sizes. Available at:. Pract Assess Res Eval, pp. 18. http://pareonline.net/getvn.asp?v=18&n=10.
DeCarolis, N.A., Rivera, P.D., Ahn, F., Amaral, W.Z., LeBlanc, J.A., Malhotra, S., Shih, H.-Y., Petrik, D., Melvin, N., Chen, B.P.C., Eisch, A.J., 2014. 56Fe particle exposure results in a long-lasting increase in a cellular index of genomic instability and transiently suppresses adult hippocampal neurogenesis in vivo. Life Sci. Space Res. 2, 70–79.
Deng, W., Aimone, J.B., Gage, F.H., 2010. New neurons and new memories: how does adult hippocampal neurogenesis affect learning and memory? Nat. Rev. Neurosci. 11, 339–350.
Dennis, C.V., Suh, L.S., Rodriguez, M.L., Kril, J.J., Sutherland, G.T., 2016. Human adult neurogenesis across the ages: an immunohistochemical study. Neuropathol. Appl. Neurobiol. 42, 621–638.
Drapeau, E., Nora Abrous, D., 2008. Stem cell review series: role of neurogenesis in age-related memory disorders. Aging Cell 7, 569–589.
Encinas, J.M., Michurina, T.V., Peunova, N., Park, J.-H., Tordo, J., Peterson, D.A., Fishell, G., Koulakov, A., Enikolopov, G., 2011. Division-coupled astrocytic differentiation and age-related depletion of neural stem cells in the adult hippocampus. Cell Stem Cell 8, 566–579.
Fanselow, M.S., Dong, H.-W., 2010. Are the dorsal and ventral hippocampus functionally distinct structures? Neuron 65, 7–19.
Farrar, C.E., Huang, C.S., Clarke, S.G., Houser, C.R., 2005. Increased cell proliferation and granule cell number in the dentate gyrus of protein repair-deficient mice. J. Comp. Neurol. 493, 524–537.
Gil-Mohapel, J., Brocardo, P.S., Choquette, W., Gothard, R., Simpson, J.M., Christie, B.R., 2013. Hippocampal neurogenesis levels predict WATERMAZE search strategies in the aging brain. PLoS One 8, e75125.
Gonçalves, J.T., Schafer, S.T., Gage, F.H., 2016. Adult neurogenesis in the Hippocampus: from stem cells to behavior. Cell 167, 897–914.
Hayes, N.L., Nowakowski, R.S., 2002. Dynamics of cell proliferation in the adult dentate gyrus of two inbred strains of mice. Brain Res. Dev. Brain Res. 134, 77–85.
Ihunwo, A.O., Tembo, L.H., Dzamalala, C., 2016. The dynamics of adult neurogenesis in human hippocampus. Neural Regen. Res. 11, 1869–1883.
Jinno, S., 2011. Topographic differences in adult neurogenesis in the mouse hippocampus: a stereology-based study using endogenous markers. Hippocampus 21, 467–480.
Kanatsou, S., Karst, H., Kortesidou, D., van den Akker, R.A., den Blaauwen, J., Harris, A.P., Seckl, J.R., Krugers, H.J., Joels, M., 2017. Overexpression of mineralocorticoid receptors in the mouse forebrain partly alleviates the effects of chronic early life stress on spatial memory, neurogenesis and synaptic function in the dentate gyrus. Front. Cell. Neurosci. 11, 132.
Kempermann, G., Kuhn, H.G., Gage, F.H., 1997a. More hippocampal neurons in adult mice living in an enriched environment. Nature 386, 493–495.
Kempermann, G., Kuhn, H.G., Gage, F.H., 1997b. Genetic influence on neurogenesis in the dentate gyrus of adult mice. Proc. Natl. Acad. Sci. U. S. A. 94, 10409–10414.
Kempermann, G., Gast, D., Kronenberg, G., Yamaguchi, M., Gage, F.H., 2003. Early determination and long-term persistence of adult-generated new neurons in the hippocampus of mice. Dev. Suppl. 130, 391–399.

Kempermann, G., Song, H., Gage, F.H., 2015. Neurogenesis in the adult Hippocampus. Cold Spring Harb. Perspect. Biol. 7 a018812.
Kriegstein, A., Alvarez-Buylla, A., 2009. The glial nature of embryonic and adult neural stem cells. Annu. Rev. Neurosci. 32, 149–184.
Kuhn, H.G., Dickinson-Anson, H., Gage, F.H., 1996. Neurogenesis in the dentate gyrus of the adult rat: age-related decrease of neuronal progenitor proliferation. J. Neurosci. Off. J. Soc. Neurosci. 16, 2027–2033.
Lee, S.W., Clemenson, G.D., Gage, F.H., 2012. New neurons in an aged brain. Behav. Brain Res. 227, 497–507.
Ming, G.-L., Song, H., 2011. Adult neurogenesis in the mammalian brain: significant answers and significant questions. Neuron 70, 687–702.
Mirescu, C., Gould, E., 2006. Stress and adult neurogenesis. Hippocampus 16, 233–238.
Morgenstern, N.A., Lombardi, G., Schinder, A.F., 2008. Newborn granule cells in the ageing dentate gyrus. J. Physiol. (Paris) 586, 3751–3757.
Moser, M.B., Moser, E.I., 1998. Functional differentiation in the hippocampus. Hippocampus 8, 608–619.
Mosher, K.I., Schaffer, D.V., 2017. Influence of hippocampal niche signals on neural stem cell functions during aging. Cell Tissue Res. 371, 115–124.
Nollet, M., Gaillard, P., Tanti, A., Girault, V., Belzung, C., Leman, S., 2012. Neurogenesis-independent antidepressant-like effects on behavior and stress axis response of a dual orexin receptor antagonist in a rodent model of depression. Neuropsychopharmacol. Off. Publ. Am. Coll. Neuropsychopharmacol. 37, 2210–2221.
O'Leary, O.F., Cryan, J.F., 2014. A ventral view on antidepressant action: roles for adult hippocampal neurogenesis along the dorsoventral axis. Trends Pharmacol. Sci. 35, 675–687.
Olariu, A., Cleaver, K.M., Cameron, H.A., 2007. Decreased neurogenesis in aged rats results from loss of granule cell precursors without lengthening of the cell cycle. J. Comp. Neurol. 501, 659–667.
Pilz, G.-A., Bottes, S., Betizeau, M., Jörg, D.J., Carta, S., Simons, B.D., Helmchen, F., Jessberger, S., 2018. Live imaging of neurogenesis in the adult mouse hippocampus. Science 359, 658–662.
Sahay, A., Hen, R., 2007. Adult hippocampal neurogenesis in depression. Nat. Neurosci. 10, 1110–1115.
Seki, T., Arai, Y., 1995. Age-related production of new granule cells in the adult dentate gyrus. Neuroreport 6, 2479–2482.
Seri, B., García-Verdugo, J.M., McEwen, B.S., Alvarez-Buylla, A., 2001. Astrocytes give rise to new neurons in the adult mammalian hippocampus. J. Neurosci. Off. J. Soc. Neurosci. 21, 7153–7160.
Smith, L.K., White, C.W., Villeda, S.A., 2017. The systemic environment: at the interface of aging and adult neurogenesis. Cell Tissue Res. 371, 105–113.
Snyder, J.S., Choe, J.S., Clifford, M.A., Jeurling, S.I., Hurley, P., Brown, A., Kamhi, J.F., Cameron, H.A., 2009a. Adult-born hippocampal neurons are more numerous, faster-maturing and more involved in behavior in rats than in mice. J. Neurosci. Off. J. Soc. Neurosci. 29, 14484–14495.
Snyder, J.S., Radik, R., Wojtowicz, J.M., Cameron, H.A., 2009b. Anatomical gradients of adult neurogenesis and activity: young neurons in the ventral dentate gyrus are activated by water maze training. Hippocampus 19, 360–370.
Sorrells, S.F., Paredes, M.F., Cebrian-Silla, A., Sandoval, K., Qi, D., Kelley, K.W., James, D., Mayer, S., Chang, J., Auguste, K.I., Chang, E.F., Gutierrez, A.J., Kriegstein, A.R., Mathern, G.W., Oldham, M.C., Huang, E.J., Garcia-Verdugo, J.M., Yang, Z., Alvarez-Buylla, A., 2018. Human hippocampal neurogenesis drops sharply in children to undetectable levels in adults. Nature 555, 377–381.
Spalding, K.L., Bergmann, O., Alkass, K., Bernard, S., Salehpour, M., Huttner, H.B., Boström, E., Westerlund, I., Vial, C., Buchholz, B.A., Possnert, G., Mash, D.C., Druid, H., Frisén, J., 2013. Dynamics of hippocampal neurogenesis in adult humans. Cell 153, 1219–1227.
Student, 1908. The probable error of a mean. Biometrika 6, 1–25.
Sui, Y., Vermeulen, R., Hökfelt, T., Horne, M.K., Stanić, D., 2013. Female mice lacking cholecystokinin 1 receptors have compromised neurogenesis, and fewer dopaminergic cells in the olfactory bulb. Front. Cell. Neurosci. 7, 13.
Tanti, A., Rainer, Q., Minier, F., Surget, A., Belzung, C., 2012. Differential environmental regulation of neurogenesis along the septo-temporal axis of the hippocampus. Neuropharmacology 63, 374–384.
Tapia-González, S., Muñoz, M.D., Cuartero, M.I., Sánchez-Capelo, A., 2013. Smad3 is required for the survival of proliferative intermediate progenitor cells in the dentate gyrus of adult mice. Cell Commun Signal CCS 11, 93.
van Praag, H., Kempermann, G., Gage, F.H., 1999. Running increases cell proliferation and neurogenesis in the adult mouse dentate gyrus. Nat. Neurosci. 2, 266–270.
Walker, T.L., Wierick, A., Sykes, A.M., Waldau, B., Corbeil, D., Carmeliet, P., Kempermann, G., 2013. Prominin-1 allows prospective isolation of neural stem cells from the adult murine Hippocampus. J. Neurosci. 33, 3010–3024.
Walter, J., Keiner, S., Witte, O.W., Redecker, C., 2011. Age-related effects on hippocampal precursor cell subpopulations and neurogenesis. Neurobiol. Aging 32, 1906–1914.
Wiget, F., van Dijk, R.M., Louet, E.R., Slomianka, L., Amrein, I., 2017. Effects of strain and species on the septo-temporal distribution of adult neurogenesis in rodents. Front. Neurosci. 11, 719.
Wu, M.V., Sahay, A., Duman, R.S., Hen, R., 2015. Functional differentiation of adult-born neurons along the septotemporal axis of the dentate gyrus. Cold Spring Harb. Perspect. Biol. 7 a018978.
Zeng, C., Pan, F., Jones, L.A., Lim, M.M., Griffin, E.A., Sheline, Y.I., Mintun, M.A., Holtzman, D.M., Mach, R.H., 2010. Evaluation of 5-ethynyl-2′-deoxyuridine staining as a sensitive and reliable method for studying cell proliferation in the adult nervous system. Brain Res. 1319C, 21–32.